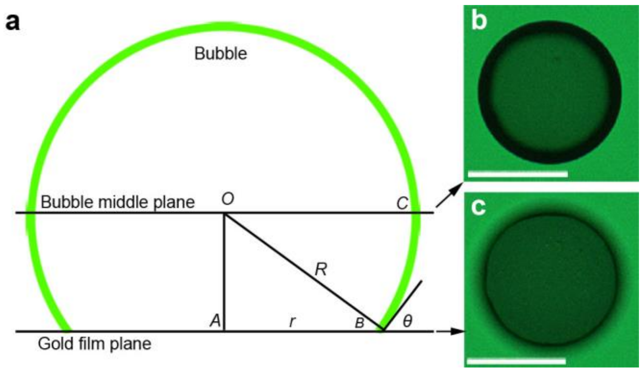

Supplementary Figure S1 | Estimation of the contact angle. (a) Schematic of the method used for estimating contact angle θ from microscopy image. (b) and (c) are the top-view images of the surface bubble in two different focal planes of the microscopy. Scale bar: 50 µm. The middle plane of the bubble was first imaged as shown in Supplementary Figure S1(b), which gives the radius R of the surface bubble. Here, R = OC = 37.1 µm. Then, the gold film plane was imaged as shown in Supplementary Figure S1(c), giving the radius r of the contact circle between the surface bubble and gold film: r = AB = 34.4 µm. Here, we define θ as the contact angle as shown in Supplementary Figure S1(a). The contact angle is estimated by θ = arcsin(r/R) = 68°.

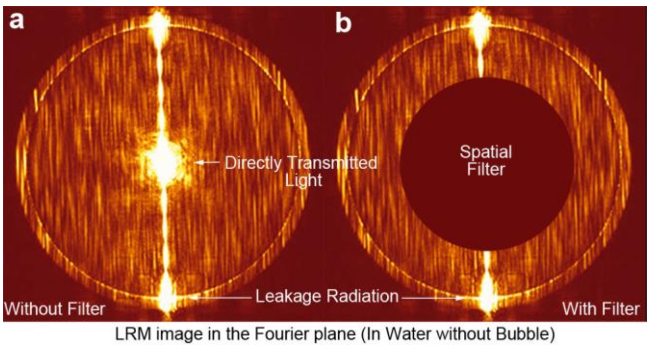

Supplementary Figure S2 | Fourier plane leakage radiation images of SPPs. (a) without and (b) with a spatial filter. The spatial filter is a home-made disk made of aluminium foil which was place in front of lens 2. The centre spot in Supplementary Figure S2(a) is the directly transmitted light through the gold film. This directly transmitted light will saturate the CCD and make it hard to distinguish the SPP field. However, it can be easily blocked by a spatial filter in the Fourier plane as shown in Supplementary Figure S2(b).

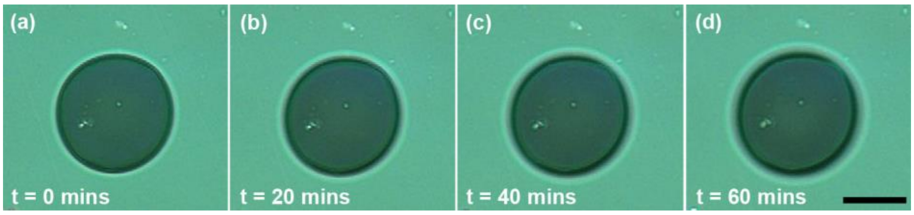

Supplementary Figure S3 | Bubble Stability. (a–d) Images of bubble shape recorded every 20 minutes maintaining laser intensity. Scale bar: 40 µm. There was very little change observed in bubble shape, maintaining a diameter of approximately 71 µm. The surface bubble can stably exist on the gold surface as long as the incident laser keeps heating the gold surface and the entire system maintains in the equilibrium state.

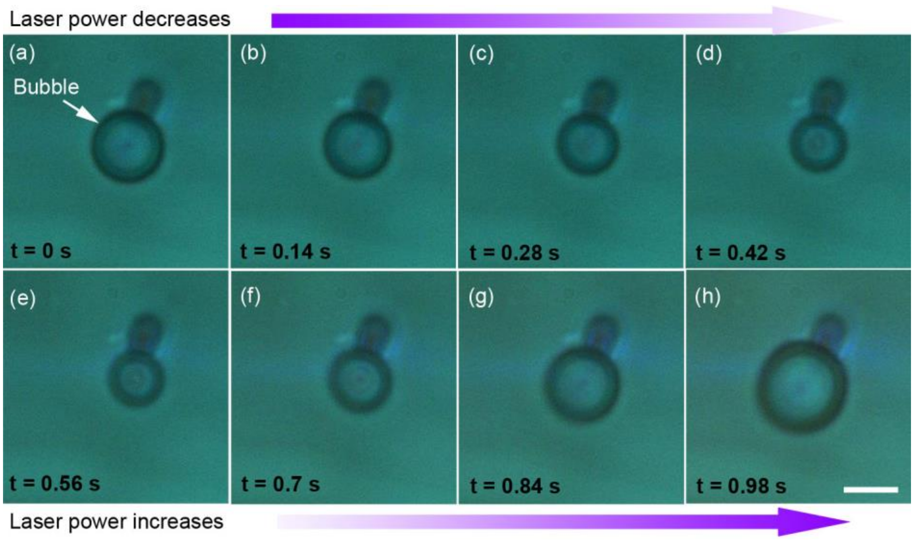

Supplementary Figure S4 | Changing bubble size by modulating laser power. (a–d) Bubble size decreases with decreasing the laser power. (e–h) Bubble size increases with increasing the laser power. The dark object adjacent to the bubble is a speck of dust on the gold film. Scale bar: 5 µm. In the experiment, the laser power was continuously varied by manually rotating a variable neutral density filter. In this way, the laser power was adjustable from 0 to 45 mW measured on the sample plane. After a surface bubble was generated on the gold film, the laser power was continuously decreased or increased by manually rotating the variable neutral density filter clockwise or counter-clockwise. The bubble contraction and expansion rates obtained from Supplementary Figure S4 are approximately 5 and 10 µm/s, respectively, and the difference is a result of manually varied tuning rates. To achieve more precise and programmable tuning, one may replace the variable neutral density filter by an electro-optic modulator (EOM). The minimal change of bubble size that can be achieved depends on how precisely the laser power can be modulated. In this experiment, the minimal change of diameter is about 350 nm.

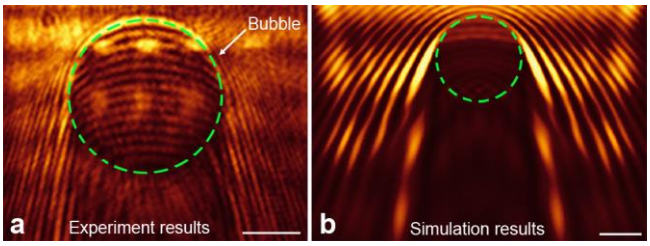

Supplementary Figure S5 | Experimental and FDTD simulation results for a surface bubble interacting with SPPs with plane wavefront. In the experimental results shown in Supplementary Figure S5(a), the straight grating used to generate SPPs with plane wave front has a width and length of 2.6 and 60 µm, respectively. The surface bubble with a diameter of 27 µm is 34 µm away from the straight grating. The green dashed circle represents the surface bubble boundary on gold film. Scale bar: 10 µm. In the simulation results shown in Supplementary Figure S5(b), a grating with a reduced width and length of 2.6 and 20 µm is used to save computation resources. The surface bubble with radius r = 5 µm on gold film is 4.5 µm away from the grating. The green dashed circle represents the surface bubble boundary on gold film. Scale bar: 5 µm.

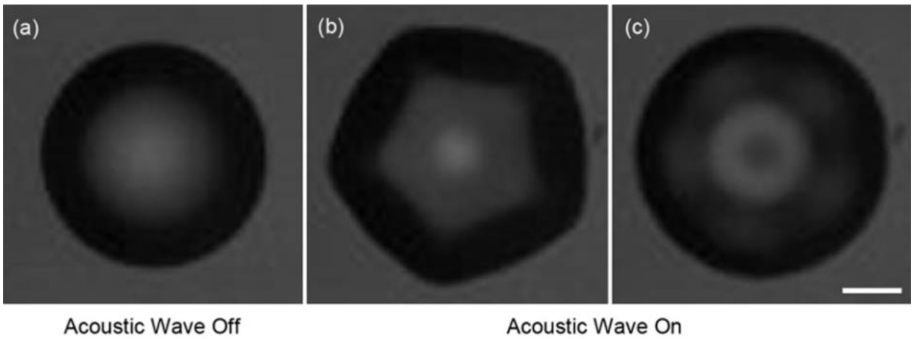

Supplementary Figure S6 | Changing the shape of surface bubble with acoustic waves. (a) Surface bubble image before applying acoustic waves. (b,c) Surface bubble image after applying acoustic waves. Scale bar: 20 µm. In the experiment, a piezo transducer was bonded to the sample surface. After a surface bubble was generated the piezo transducer was actuated at a frequency of 106 kHz and an amplitude of 10 V peak-to-peak to generate acoustic waves. The bubble surface vibrates with the acoustic waves and was imaged with a fast camera. Supplementary Figure S6(a) shows a surface bubble with a diameter of 75 µm without turning on the acoustic waves. Supplementary Figures S6(b) and (c) are two instantaneous images after applying the acoustic waves on the surface bubble. The bubble oscillates near the 5th harmonic mode. It clearly shows that acoustic waves can be used to dynamically change the shape of surface bubble.

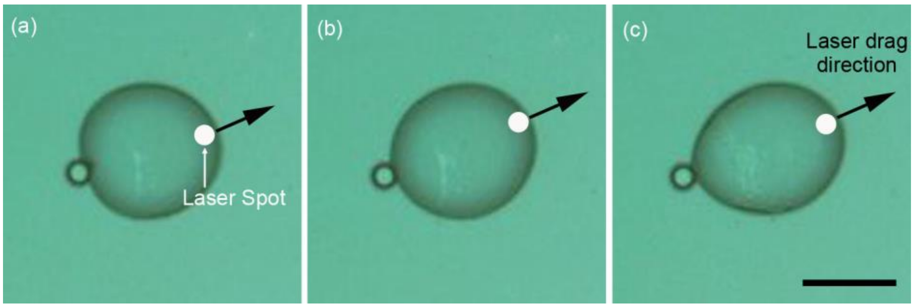

Supplementary Figure S7 | Changing surface bubble shape by moving laser spot. (a) – (c) Shape of surface bubble evolves as the laser spot moves. The white solid circle is the laser spot and the black arrow shows the laser's direction of motion. Scale bar: 50 μm. In the experiment, the left side of the bubble was fixed on the gold film by surface tension between the bubble and a discontinuous structure on the gold film (a polystyrene bead that was stuck on the gold film). When the laser spot moves along the direction indicated by a black arrow in Supplementary Figure S7, the right front surface of the bubble is dragged and moves with the laser spot. In this way, the curvature of the surface bubble can be dynamically changed to achieve different functionality. The polystyrene bead was used here to demonstrate the working principle. It can be readily replaced by another laser spot which moves in the opposite direction from the first one. In fact, the bubble shape can be changed into a more complex shape by stretching its boundary on the gold film with laser spot arrays that are modulated by a spatial light modulator.

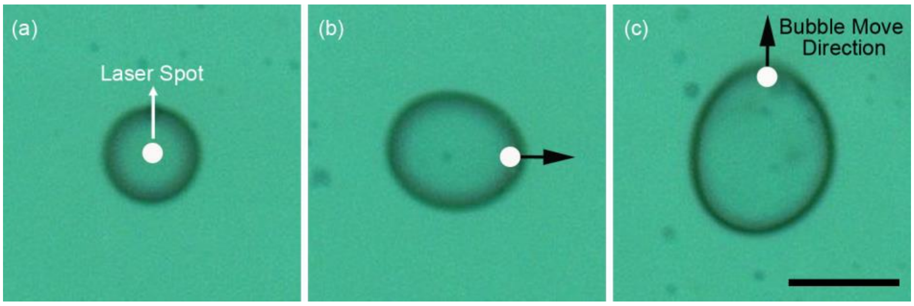

Supplementary Figure S8 | Changing the shape of surface bubble by moving laser spot. (a) Surface bubble with spherical shape. (b) – (c) Bubble shape evolves as laser spot (marked as a white circle) moves on the gold film in the direction marked as a black arrow. Scale bar: 50 μm. A surface bubble with spherical shape was generated on the gold-water interface as shown in Supplementary Figure S8(a). Then the laser spot moves on the gold film along the direction marked by a black arrow as shown in Supplementary Figure S8(b) and (c). The bubble follows the movement of the laser spot and was stretched into different shapes by the drag force (caused by the surface tension between the bubble and gold film) exerted on the bubble with direction opposite to the direction of motion. Alternatively, the flow of fluids can change the bubble shape in a similar fashion.

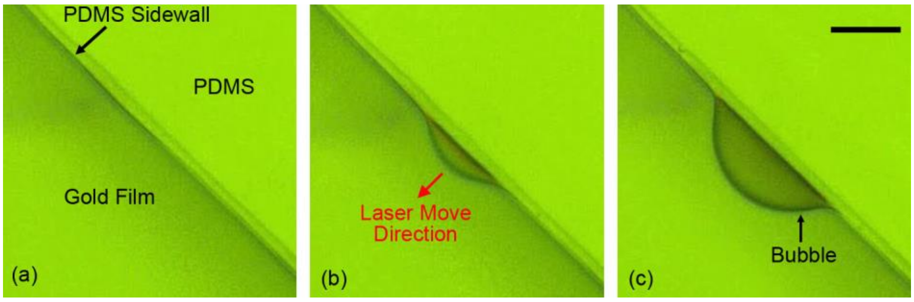

Supplementary Figure S9 | Shaping surface bubble with microchannel and laser spot. (a) Micro-channel on gold film. The straight line is the sidewall of the PDMS channel. (b)–(c) Changing bubble shape as a result of moving the laser spot. Scale bar: 20 μm. A microchannel made of PDMS was place on top of the gold film as shown in Supplementary Figure S9(a). The straight line in the figure is the sidewall of the PDMS channel. A surface bubble was generated between PDMS sidewall and gold film. The right side of the surface bubble was attached to the PDMS sidewall due to surface tension and the left side was dragged by the laser spot as marked by the red arrow in Supplementary Figure S9(b). In this way the bubble forms a parabolic shape. The curvature of the bubble can be further changed by moving the laser spot as shown in Supplementary Figure S9(c).

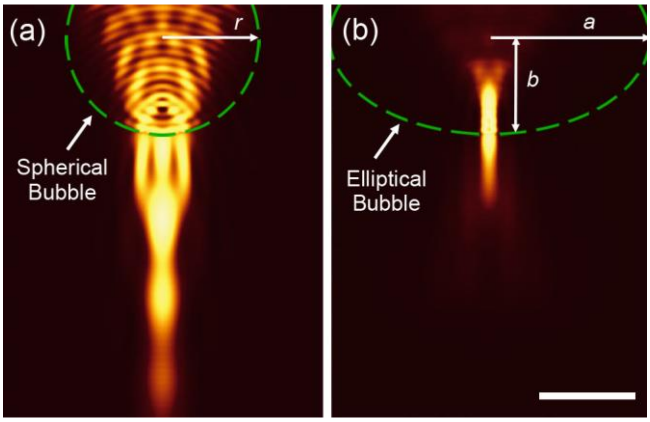

Supplementary Figure S10 | FDTD simulation results for plasmofluidic lenses with a spherical and an elliptical shape. (a) SPP field after passing through a spherical surface bubble. The radius of the surface bubble is r = 5 μm. (b) SPP field after passing through an elliptical surface bubble. The major and minor radius are a = 8 μm and b = 5 μm, respectively. The green dashed curve represents the surface bubble boundary on gold film. Scale bar: 5 μm. SPPs are well collimated by a plasmofluidic lens with a spherical shape as shown in Supplementary Figure S10(a). The spherical plasmofluidic lens acts as a SPP collimator. In contrast, SPPs are well focused by an elliptical-shaped plasmofluidic lens as shown in Supplementary Figure S10(b). The plasmofluidic lens acts as an aspheric lens in this case.